

A SPECTRAL METHOD FOR INTEGRAL FORMULATIONS OF MEDIUM-FREQUENCY SCATTERING PROBLEMS

JOHANNES TAUSCH[†]

Abstract. A fast method for the computation of layer potentials that arise in acoustic scattering is introduced. The principal idea is to split the singular kernel into a smooth and a local part. The potential due to the smooth part is computed efficiently using non-equispaced FFTs, the potential due to the local part is expanded as a series in the mollification parameter. The complexity of the approach is shown to be $O(n + \kappa^3 \log \kappa)$, where n is the number of degrees of freedom in the discretization and κ is the wave number. The constant factor in this asymptotic estimate is small since no singular surface integrals must be computed. Therefore the method is particularly efficient for medium-sized scatterers (50-100 wavelengths) that may have complicated geometry.

Key words. Boundary Element Method, Helmholtz Equation, Fast Method, Scattering.

AMS subject classifications. 65N38, 65T50, 65Y20

1. Introduction. It is commonly accepted that the boundary element method is an effective approach to solve the Helmholtz equation in the exterior of a scatterer. It has the advantage that only the finite boundary surface has to be discretized and that the radiation condition is automatically satisfied. In the recent past a variety of methods have been developed to handle the dense matrices associated with discretized layer potentials. These can be roughly classified into two groups, namely hierarchical and grid-based methods.

Examples of hierarchical methods are the Fast Multipole Method[9], hierarchical matrices[2] and wavelets[1]. These methods are based on clustering interactions between panels in a hierarchical manner; the larger the separation, the larger the clusters. The efficiency and accuracy of these methods depends critically on how the cluster interactions can be approximated by low-rank matrices. In the case of boundary integral operators associated with the Laplace, Stokes or Lamé equations asymptotically optimal schemes have been developed. That is, the complexity of a matrix-vector multiplication is order n , or order $n \log^p n$, while the convergence rate of the discretization scheme is preserved, see, e.g. [17, 16, 19].

In the case of the Helmholtz equation, the size of the scatterer, measured in wavelengths, is the dominant factor that influences computational cost and accuracy. It is well known that in the high-frequency regime large clusters are no longer approximated by low-rank matrices, and therefore the efficiency of the aforementioned methods breaks down. To overcome this problem it has been proposed to use the Fast Multipole Method with diagonal translation operators, [15]. This technique has been extended in [6, 18].

A different approach that avoids large clusters is to replace the surface distribution by equivalent sources on a uniform grid. The fast Fourier transform can be employed to compute grid potentials efficiently. Since the grid is only accurate when the source and the evaluation point are well separated, the nearby interactions must be computed directly, by adding up contributions of individual sources. Grid-based methods are quite popular even though it appears that the asymptotic complexity is generally higher than what can be achieved with hierarchical methods. However, in many engineering applications the geometry is complicated and the mesh is relatively coarse, therefore constant factors often play an important role. Applications of

[†]Department of Mathematics, Southern Methodist University, Dallas, TX 75275, tauschk@smu.edu

grid-based methods for the Laplace equation can be found in [11, 14] for elasticity in [13]. For high-frequency scattering this methodology, combined with local high-order discretizations have been described in [4].

If the scatterer is smooth and isomorphic to a sphere, spectral element methods, based on expansion of the solution into spherical harmonics have been shown to be successful [8].

The approach described in this paper is closer to grid-based methods in that FFTs are used to accelerate the matrix-vector product. However, there is no uniform grid with equivalent charges. The idea here is to split the Green's function into a smooth approximation and a singular, essentially local part. The smooth part of the Green's function is replaced by a rapidly converging Fourier series. We will show how non-equispaced FFTs can be used to compute layer potentials with such a kernel effectively. A similar idea has been applied earlier to the heat equation [10].

The local part can be evaluated using expansions with respect to the mollification parameter. Thus the computation of the local part amounts to multiplying with a diagonal matrix. Since there is no need to compute the nearfield directly, we believe that the discussed approach is competitive with hierarchical and grid-based methods.

We will discuss how the mollification parameter and the number of Fourier modes have to be selected as a function of the meshwidth and the wave number to obtain efficient and accurate schemes. Our analysis is based on bounding the error of the bilinear form when the wave number is increased. It should be noted that this does not give estimates of the error of the solution. For that, realistic estimates of constants in the inf-sup condition are necessary, which are not available. However, we will present numerical examples that suggest that the selection strategy of the parameters indeed control the error when increasing the wavenumber.

2. Problem Formulation. For simplicity of exposition, the focus of this paper will be on the sound-soft acoustic scattering of an incoming field u^{inc} of a smooth obstacle $D \subset \mathbf{R}^3$. The reflected field u is described by the Dirichlet problem to the Helmholtz equation with the Sommerfeld radiation condition

$$(2.1) \quad \begin{aligned} \Delta u(x) + \kappa^2 u(x) &= 0, & x \in \mathbf{R}^3 \setminus D \\ u(x) &= -u^{\text{inc}}(x), & x \in S := \partial D \\ \frac{\partial u}{\partial r} - i\kappa u &= O\left(\frac{1}{\|x\|^2}\right). \end{aligned}$$

Here, κ is the wave number. We assume that the problem is scaled such that the scatterer is located inside a cube of side length $1 - d$, that is

$$(2.2) \quad S \subset [0, 1 - d]^3$$

where $0 < d \ll 1$ is a constant.

A classical approach to treat the Helmholtz problem (2.1) is the combined layer ansatz of Brakhage and Werner [3], where the scattered field is represented by a combination of a single- and double layer potential

$$(2.3) \quad u(x) = (\mathcal{K} - i\eta\mathcal{V})\sigma(x), \quad x \in \mathbf{R}^3 \setminus \overline{D},$$

where $\eta > 0$ is the coupling parameter, σ an unknown surface density and

$$(2.4) \quad \mathcal{V}\sigma(x) := \int_S \frac{\exp(i\kappa\|x - y\|)}{4\pi\|x - y\|} \sigma(y) dS_y,$$

$$(2.5) \quad \mathcal{K}\sigma(x) := \int_S \frac{\partial}{\partial n_y} \frac{\exp(i\kappa\|x - y\|)}{4\pi\|x - y\|} \sigma(y) dS_y$$

are the single and double layer operator, respectively. By letting $x \rightarrow S$ from the exterior of the scatterer, and taking the jump relations of layer potentials under consideration, the following boundary integral equation for σ can be derived

$$(2.6) \quad \frac{1}{2}\sigma(x) + (\mathcal{K} - i\eta\mathcal{V})\sigma(x) = -u^{\text{inc}}(x), \quad x \in S.$$

It is well known that (2.6) is a well posed problem when $\eta > 0$, see, e.g., [5].

To obtain a discretization of (2.6) we introduce the space X_h of piecewise polynomial functions on a triangulation of S . This triangulation is assumed to be quasi-uniform and the maximal diameter of a triangle is denoted by h . The nodal basis $\{\varphi_i\}$, $i = 1, \dots, n$ of X_h consists of functions with local support. Note that $n = O(h^{-2})$. The Galerkin approximation is defined to be the function $\sigma_h \in X_h$ whose residual is $L^2(S)$ -orthogonal to X_h . This leads to the linear system $(M + A)x = b$, where the coefficients of the system matrix and the right hand side are given, respectively, by

$$\begin{aligned} M_{i,j} &= \frac{1}{2} \int_S \varphi_i(x) \varphi_j(x) dS_x \\ A_{i,j} &= \int_S \int_S \left(\frac{\partial}{\partial n_y} - i\eta \right) \frac{\exp(i\kappa\|x-y\|)}{4\pi\|x-y\|} \varphi_i(x) \varphi_j(y) dS_y dS_x, \\ b_i &= - \int_S \varphi_i(x) u^{\text{inc}}(x) dS_x. \end{aligned}$$

Since this system is large, iterative methods for its solution must be employed. The dominant cost in such a scheme is the multiplication of a vector with the dense matrix A , which, if it is done in the obvious way, has $O(n^2)$ complexity. The article will discuss a scheme to compute the product approximately with a highly reduced flop count.

3. Splitting of the Helmholtz Kernel. The heart of the method is the splitting of the Helmholtz kernel

$$(3.1) \quad G(r) = G_\delta(r) + E_\delta(r)$$

into a smooth part $G_\delta(r)$ and a singular, local part $E_\delta(r)$. Here, δ is the mollification parameter that controls the smoothness of G_δ . This splitting results in a splitting of the single layer potential

$$\mathcal{V}g(x) = \Phi^S(x) + \Phi^L(x)$$

where

$$(3.2) \quad \Phi^S(x) = \int_S G_\delta(x-y)g(y) dS_y$$

$$(3.3) \quad \Phi^L(x) = \int_S E_\delta(x-y)g(y) dS_y$$

The splitting of the double layer potential $\mathcal{K}g(x) = \Psi^S(x) + \Psi^L(x)$ is defined analogously.

3.1. Smooth Part. The Green's function can be expressed in Fourier space,

$$(3.4) \quad G(r) = \frac{\exp(i\kappa\|r\|)}{4\pi\|r\|} = \frac{1}{(2\pi)^3} \int_{\mathbb{R}^3} \frac{1}{\|\omega\|^2 - \kappa^2} \exp(ir \cdot \omega) d^3\omega.$$

Exploiting the spherical symmetry of the Fourier transform leads to

$$(3.5) \quad G(r) = \frac{1}{2\pi^2} \int_0^\infty \frac{\rho^2}{\rho^2 - \kappa^2} j_0(\rho\|r\|) d\rho$$

where $j_0(z) = \sin(z)/z$ is the spherical Bessel function of order zero. The integral in (3.5) is understood in the sense that the singularity at $\rho = \kappa$ is circumvented in lower complex half-plane, thereby enforcing the Sommerfeld radiation condition, see, e.g., [7].

The decay rate of the transform at infinity determines the regularity of the kernel. The integrand in (3.5) is only $O(\rho^{-1})$ as $\rho \rightarrow \infty$ which explains the singularity of the Green's function in the origin. A smooth approximation of the kernel can be obtained by multiplying the transform with a filter to increase the decay rate at infinity

$$(3.6) \quad G_\delta(r) = \frac{1}{2\pi^2} \int_0^\infty H(\delta(\rho^2 - \kappa^2)) \frac{\rho^2}{\rho^2 - \kappa^2} j_0(\rho\|r\|) d\rho$$

where H is the filter. Because of the singularity of the integrand at $\rho = \kappa$ it is more convenient to write the filter in the form as it appears in (3.6) and not as $H(\delta\rho^2)$.

There are several possible choices for H . If the filter is a rational function, then G_δ can be expressed in closed form. To that end, write the filter in partial fraction decomposition

$$H(z) = \sum_{k=1}^q \frac{c_k}{z + w_k^2},$$

where the coefficients w_k and c_k are at our disposition. It will become clear later that because of the singularity of the integrand it is necessary that

$$(3.7) \quad H(0) = 1.$$

Basic complex variable arguments show that

$$(3.8) \quad \frac{H(z)}{z} = \sum_{k=0}^q \frac{d_k}{z + w_k^2}.$$

where $w_0 = 0$ and because of condition (3.7)

$$(3.9) \quad d_0 = 1 \quad \text{and} \quad d_k = \frac{c_k}{w_k^2}.$$

Substitution of (3.8) into (3.6) and the change variables $\rho \rightarrow \sqrt{\delta}\rho$ leads to

$$G_\delta(r) = \frac{1}{2\pi^2\sqrt{\delta}} \sum_{k=0}^q d_k \int_0^\infty \frac{\rho^2}{\rho^2 - \tilde{w}_k^2} j_0\left(\rho \frac{\|r\|}{\sqrt{\delta}}\right) d\rho,$$

where

$$(3.10) \quad \tilde{\kappa} = \sqrt{\delta}\kappa \quad \text{and} \quad \tilde{w}_k = \sqrt{\tilde{\kappa}^2 - w_k^2}$$

The integrals in the last expression are of the same form as (3.5). Therefore the mollified Green's function has the closed form

$$(3.11) \quad G_\delta(r) = \frac{\exp(i\kappa\|r\|)}{4\pi\|r\|} + \sum_{k=1}^q d_k \frac{\exp(i\tilde{w}_k\|r\|/\sqrt{\delta})}{4\pi\|r\|}$$

In the discussion below, it will be convenient to write the decomposition in (3.11) in the form

$$(3.12) \quad G(r) = G_\delta(r) + \frac{1}{\sqrt{\delta}} E\left(\frac{\|r\|}{\sqrt{\delta}}\right)$$

where E is singular at $z = 0$ given by

$$(3.13) \quad E(z) = - \sum_{k=1}^q d_k \frac{\exp(i\tilde{w}_k z)}{4\pi z}.$$

A good filter must satisfy two properties. First, it must decay rapidly to ensure smoothness, that is, there must be a constant c such that

$$(3.14) \quad |H(z)| \leq c \min(1, z^{-q}).$$

Second, the kernel E must decay exponentially away from the origin, this is why it will be referred to as the local part. To ensure the latter condition, it is necessary that $\text{Im}(\tilde{w}_k)$ is bounded away from zero as $\kappa \rightarrow \infty$. If w_k is real, then (3.10) implies that

$$(3.15) \quad \sqrt{\delta} < \frac{1}{\kappa} \min_{k>0} |w_k|.$$

The latter condition implies that $\tilde{\kappa}$ is bounded as $\kappa \rightarrow \infty$.

An example of a filter that satisfies (3.14) is given by

$$(3.16) \quad H(z) = \prod_{k=1}^q \frac{1}{k+z},$$

This filter has poles $w_k = i\sqrt{k}$, $k = 1, \dots, q$. Condition (3.15) is equivalent to $\sqrt{\delta} < 1/\kappa$. The filter

$$(3.17) \quad H(z) = \frac{1}{(1+z)^q}$$

also satisfies the decay property. Because of the repeated poles, the smooth part corresponding to this filter is slightly different from (3.11):

$$G_\delta(r) = \frac{\exp(i\kappa\|r\|)}{4\pi\|r\|} + p\left(\frac{\|r\|}{\sqrt{\delta}}\right) \frac{\exp(i\tilde{w}\|r\|/\sqrt{\delta})}{\|r\|}.$$

Here $p(\cdot)$ is a polynomial of degree $q-1$ and $\tilde{w} = \sqrt{1-\delta\kappa^2}$. As with the previous filter, condition (3.15) is $\sqrt{\delta} < 1/\kappa$.

3.2. Local Part. The smooth part is a good approximation of the actual Green's function if δ is small and r is large. In the neighborhood of the origin the two functions are very different and therefore the contribution of the local part must be accounted for. In this section we show that the local part has an expansion with respect to the mollification parameter $\sqrt{\delta}$ and show how to compute the expansion coefficients.

Since condition (3.15) implies that the coefficients \tilde{w}_k in (3.13) have a positive imaginary part, the function E_δ decays exponentially away from the origin. We introduce the smooth cut-off function $\tilde{\chi}$ for some $0 < \nu < 1$ which is small enough

such that the surface has a parameterization of the form $y(t) = x + At + nh(t)$ in the ν -neighborhood of x . Here n is the normal of the surface at the point x , $A \in \mathbb{R}^{3 \times 2}$ has two orthogonal columns that span the tangent plane at x and $h(t) = O(|t|^2)$ is some scalar function in $t \in \mathbb{R}^2$. The local single-layer potential $\Phi_\delta(x)$ in (3.3) can be written in the form

$$\begin{aligned} \Phi_\delta(x) &= \int_S E_\delta(x-y)g(y) dS_y \\ &= \int_S E_\delta(x-y)\tilde{\chi}_\nu(x-y)g(y) dS_y + O\left(\exp\left(-\frac{\nu}{\delta}\right)\right) \\ (3.18) \quad &= \int_{\mathbb{R}^2} E_\delta(t)\tilde{g}(t)d^2t + O\left(\exp\left(-\frac{\nu}{\delta}\right)\right). \end{aligned}$$

Here, $E_\delta(t) = E_\delta(x-y(t))$, $\tilde{g}(t) = \tilde{\chi}_\nu(x-y(t))g(t)J(t)$ and $J(t)$ is the Jacobian of the parameterization. For simplicity of the argument we assume that the function $h(t)$ in the parameterization of the surface is analytic, that is,

$$(3.19) \quad h(t) = \sum_{|\alpha| \geq 2} h_\alpha t^\alpha.$$

Thus there are there are C^∞ -functions H_n such that

$$(3.20) \quad r(t) := \|x - y(t)\| = \|t\| \sum_{n=0}^{\infty} \|t\|^n H_n(\hat{t})$$

where $\hat{t} := t/|t|$ and $H_0(\hat{t}) = 1$ and $H_1(\hat{t}) = 0$. Substituting (3.20) into (3.18) leads to

$$(3.21) \quad \Phi_\delta(x) = \frac{1}{\sqrt{\delta}} \int_{\mathbb{R}^2} E\left(\frac{r(t)}{\sqrt{\delta}}\right) \tilde{g}(t) d^2t + O\left(\exp\left(-\frac{\nu}{\delta}\right)\right)$$

$$(3.22) \quad = \sqrt{\delta} \int_{\mathbb{R}^2} E\left(|t| \sum_{n=0}^{\infty} (\sqrt{\delta}|t|)^n H_n(\hat{t})\right) \tilde{g}(\sqrt{\delta}t) d^2t + O\left(\exp\left(-\frac{\nu}{\delta}\right)\right)$$

where the second integral is the result of the change of variables $t \mapsto t/\sqrt{\delta}$. The integral as a function of $\sqrt{\delta}$ is C^∞ , and can therefore be expanded in a Taylor series. The expansion coefficients are derivatives of the integral with respect to $\sqrt{\delta}$. We see that

$$(3.23) \quad \Phi_\delta(x) = \delta^{\frac{1}{2}} \Phi_0 g(x) + O(\delta^{\frac{3}{2}})$$

where

$$\Phi_0 = \int_{\mathbb{R}^2} E(\|t\|)d^2t = \frac{\pi}{i} \sum_{k=1}^q \frac{d_k}{w_k}.$$

The double layer potential is given by

$$\Psi_\delta(x) = -\frac{1}{\delta} \int_S E'\left(\frac{\|x-y\|}{\sqrt{\delta}}\right) \frac{(x-y) \cdot n_y}{\|x-y\|} g(y) dS_y.$$

The second factor of the kernel can be expanded in a similar manner as (3.20), we find that

$$\frac{(x-y) \cdot n_y}{\|x-y\|} = -\|t\| (h_{02} \cos^2 \theta + h_{11} \cos \theta \sin \theta + h_{20} \sin^2 \theta) + O(\|t\|^2)$$

where θ is the angular coordinate of t and the h 's are from expansion (3.19). Proceeding in a similar manner as for the single layer operator the following expansion follows

$$(3.24) \quad \Psi_\delta(x) = \delta^{\frac{1}{2}} \Psi_0 g(x) + O(\delta^{\frac{3}{2}})$$

where

$$\Psi_0 = -\frac{\pi}{i} (h_{02} + h_{20}) \sum_{k=1}^q \frac{d_k}{w_k}.$$

4. A fast algorithm for smooth, periodic kernels. We describe a fast algorithm for the smooth part of the single layer in (3.2), which is based on Fourier analysis. Modifications for the double layer are minimal and mentioned at the end of the section. For rapid convergence of the Fourier series it is necessary to multiply the smooth kernel with a sufficiently smooth cut-off function $G^S := \chi G_\delta$ that is unity inside the cube $[-1+d, 1-d]^3$ and vanishes outside $[-1, 1]^3$. Recall that we assumed in (2.2) that the surface is contained in $[0, 1-d]^3$, thus the cut-off function has no effect in the integral, and the smooth part is given by

$$(4.1) \quad \Phi^S(x) = \int_S G^S(x-y) g(y) dS_y, \quad x \in S.$$

The kernel G^S can be approximated by the truncated Fourier series G_N

$$(4.2) \quad G_N(r) := \sum_{\|k\|_\infty \leq N} \widehat{G}_k \exp(\pi i k^T r), \quad r \in [-1, 1]^3$$

where the summation index k is in \mathbb{Z}^3 . The resulting approximate potential is given by

$$(4.3) \quad \Phi_N(x) = \int_S G_N(x-y) g(y) dS_y = \sum_{\|k\|_\infty \leq N} \exp(\pi i k \cdot x) \widehat{d}_k$$

where $\widehat{d}_k = \widehat{G}_k \widehat{g}_k$ and

$$(4.4) \quad \widehat{G}_k = \frac{1}{8} \int_{[-1, 1]^3} \exp(-\pi i k \cdot r) G^S(r) d^3 r,$$

$$(4.5) \quad \widehat{g}_k = \int_S \exp(-\pi i k \cdot y) g(y) dS_y.$$

In case the smooth part of the double layer is to be calculated, the coefficients \widehat{g}_k must be replaced by

$$(4.6) \quad \widehat{g}_k = \int_S \frac{\partial}{\partial n_y} \exp(-\pi i k \cdot y) g(y) dS_y.$$

To simplify the discussion, our notations will not distinguish between the coefficients in (4.5) and (4.6). In summary, the potential computation of the potential due to the smooth parts consists of three stages. in (4.3).

1. Compute the Fourier coefficients \widehat{g}_k in (4.5).
2. Multiply $\widehat{d}_k := \widehat{G}_k \widehat{g}_k$ for $\|k\|_\infty \leq N$.

3. Evaluate the Fourier series (4.3) for $x \in S$.

The choice of the truncation parameter N depends on the wave number and the mollification parameter and can be much smaller than the linear system size n . In Section 5 the exact dependence will be investigated. Stage 2 obviously involves $O(N^3)$ operations, the other two stages can be executed efficiently using non equispaced Fast Fourier Transforms. This will be discussed next.

4.1. Computation of the \hat{g}_k 's. In this section we describe how FFTs can be used to efficiently compute the Fourier coefficients of the function g . To that end, the three-space is divided into small cubes C_l , $l = (l_1, l_2, l_3) \in \mathbb{Z}^3$, $0 \leq l_j < N$. These cubes have centers $x_l = l/N$ and side length $1/N$. Note that N is the same as in (4.2) and therefore the cubes get smaller if more terms in the Fourier series expansion of the Green's function are retained. Because of assumption (2.2) S is contained in the union of all cubes and set $S_l = C_l \cap S$ to denote the piece of the surface that intersects with the l th cube, c.f. Figure 4.1.

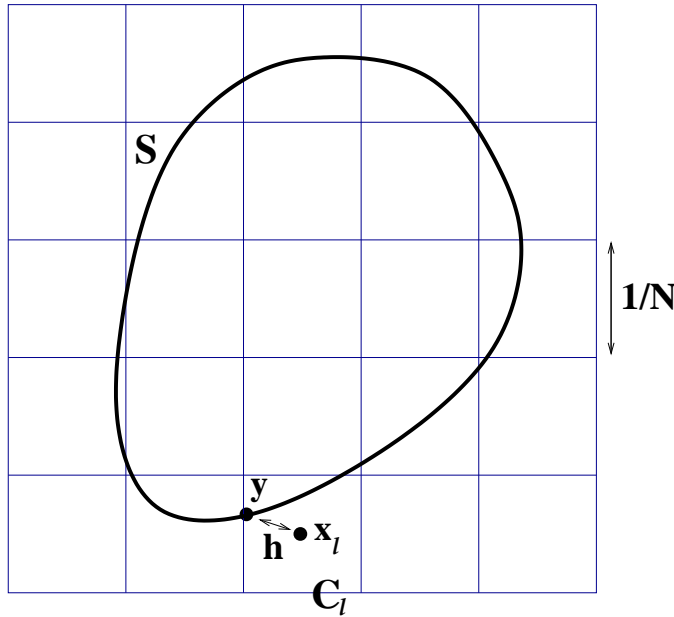


FIG. 4.1. Two dimensional illustration of the geometry.

From (4.5) it follows that the Fourier coefficients of g can be written as

$$(4.7) \quad \hat{g}_k = \sum_{\|l\|_\infty \leq N} \exp\left(\frac{-\pi i k \cdot l}{N}\right) \int_{S_l} \exp(-\pi i k \cdot (y - x_l)) g(y) dS_y.$$

The frequency and the spatial variable in the integral can be separated using the Jacobi-Anger expansion

$$\exp(-i\xi t) = \sum_{\nu=0}^{\infty} (-i)^\nu (2\nu + 1) j_\nu(\xi) P_\nu(t), \quad -1 \leq t \leq 1,$$

see, e.g., [12]. Here, $j_\nu(\cdot)$ is the spherical Bessel function of order ν and $P_\nu(\cdot)$ is the Legendre polynomial of degree ν . This formula generalizes to the three-variate case

and can be applied to the integrand in (4.7)

$$(4.8) \quad \exp(-\pi i k \cdot (y - x_l)) \approx \sum_{|\alpha| \leq p} (-i)^{|\alpha|} (2\alpha + 1) j_\alpha(\pi k H) P_\alpha\left(\frac{y - x_l}{H}\right)$$

where p is the expansion order, $H = 1/(2N)$, $\alpha = (\alpha_1, \alpha_2, \alpha_3)$ is a multi-index, $|\alpha| = \alpha_1 + \alpha_2 + \alpha_3$, $j_\alpha(x) = j_{\alpha_1}(x_1)j_{\alpha_2}(x_2)j_{\alpha_3}(x_3)$ and $P_\alpha(x)$ is defined similarly. Substitution of (4.8) into (4.7) leads to the approximation

$$\hat{g}_k \approx \sum_{|\alpha| \leq p} (-i)^\alpha (2\alpha + 1) j_\alpha(\pi k H) \sum_{\|l\|_\infty \leq N} \exp\left(\frac{-\pi i k \cdot l}{N}\right) m_l^\alpha(g),$$

where

$$(4.9) \quad m_l^\alpha(g) = \int_{S_l} P_\alpha\left(\frac{y - x_l}{H}\right) g(y) dS_y$$

is a moment for which exact formulas can be derived if the function and the surface are discretized. In particular, if g is a piecewise polynomial, then the moments are linear transformations of the coefficients of g corresponding to the nodal basis. The matrix that maps the coefficients to the α -th moments is denoted by M_α . The number of nonzero entries in M_α is n .

In matrix form, the (approximate) coefficient vector \hat{g} is given by

$$(4.10) \quad \hat{g} = \sum_{|\alpha| \leq p} K_\alpha F M_\alpha \vec{g},$$

where F is the $2N$ -long three-dimensional discrete Fourier transform, \vec{g} the vector of coefficients of g and K_α is a diagonal matrix with the factors $(-i)^{|\alpha|} (2\alpha + 1) j_\alpha(\pi k H)$. The computation of \hat{g} involves $(p+1)(p+2)(p+3)/6$ FFTs. In Section 6 we will show that it suffices to use a small value of p .

4.2. Evaluation the Fourier series. In the Galerkin discretization, the i -th component of the matrix-vector product Φ_i is the inner product of the potential Φ in (4.1) with the i -th nodal basis function φ_i . For the fast method, the potential is replaced with the approximated potential Φ_N in (4.3). In order to evaluate the potential efficiently, the Jacobi-Anger approximation (4.8) is used again, in a very similar manner as in the previous section. This is shown in the following computation

$$\begin{aligned} \Phi_i &= \int_S \varphi_i(x) \Phi_N(x) dS_x \\ &= \sum_{\|k\|_\infty \leq N} \exp\left(\frac{\pi i k \cdot l}{N}\right) \int_S \exp(\pi i k \cdot (y - x_l)) \varphi_i(x) dS_x d_k \\ &\approx \sum_{|\alpha| \leq p} \sum_{\|k\|_\infty \leq N} \exp\left(\frac{\pi i k \cdot l}{N}\right) i^{|\alpha|} (2\alpha + 1) j_\alpha(\pi k H) m_l^\alpha(\varphi_i) d_k. \end{aligned}$$

In matrix notation, the above can be written as

$$(4.11) \quad \vec{\Phi} = \sum_{|\alpha| \leq p} M_\alpha^T F^* K_\alpha \vec{d}.$$

Hence $(p+1)(p+2)(p+3)/6$ FFTs are necessary to compute the vector $\vec{\Phi}$. Furthermore, it is evident that the operation (4.11) is the adjoint of operation (4.10).

5. Error Analysis. In this section we derive estimates for the error of the bilinear form introduced when the mollified kernel corresponding to the single layer operator is replaced by the truncated Fourier series expansion. To keep the technical level of the discussion at a minimum we omit the discussion of the double layer operator, because it is completely analogous to the single layer. The main concern is the situation where $\kappa \rightarrow \infty$ and our goal is to determine N and p as a function of the wavenumber such that the resulting error remains bounded.

It is straightforward to see that

$$\langle f, (\mathcal{A} - \mathcal{A}_N)g \rangle = \sum_{\|k\|_\infty > N} \widehat{G}_k \widehat{f}_k \widehat{g}_k$$

where \mathcal{A} is the surface integral operator with kernel G^S , \mathcal{A}_N its Fourier series approximation, \widehat{G}_k are the Fourier coefficients of G and $\widehat{f}_k, \widehat{g}_k$ are the Fourier coefficients of surface distributions as defined in (4.5). The obvious way to estimate the error is

$$\begin{aligned} |\langle f, (\mathcal{A} - \mathcal{A}_N)g \rangle| &\leq \sum_{\|k\|_\infty > N} \left| \widehat{G}_k \right| \sup_k |\widehat{f}_k| \sup_k |\widehat{g}_k| \\ (5.1) \qquad \qquad \qquad &\leq \sum_{\|k\|_\infty > N} \left| \widehat{G}_k \right| \|f\|_{L^2(S)} \|g\|_{L^2(S)}. \end{aligned}$$

It is not possible to work with l_2 -estimates of \widehat{f}_k , because f can be regarded as surface-delta function in \mathbb{R}^3 which cannot be bounded by the L^2 -norm. Thus the Fourier coefficients of the kernel must be estimated in the l_1 -norm which amounts to an estimate in the $L_{[-1,1]^3}^\infty$ -norm.

The Fourier coefficients can be related to the derivatives of the function with the standard integration-by-parts argument. Since the kernel is a spherically symmetric, three-variate function, it is convenient to work with the Laplacian and the Green's formula. Because of $\Delta \exp(ik \cdot r) = -\|k\|^2 \exp(ik \cdot r)$ it follows that

$$\begin{aligned} \widehat{G}_k &= \frac{1}{8} \int_{[-1,1]^3} G_\delta(r) \chi(r) d^3 r \\ &= \frac{1}{8\|k\|^{2m}} \int_{[-1,1]^3} \Delta^m (G_\delta(r) \chi(r)) d^3 r = \frac{1}{\|k\|^{2m}} [\Delta^m (\widehat{G_\delta \chi})]_k, \end{aligned}$$

for any integer m for which the right-hand side is defined. With this estimate at hand, one obtains

$$\begin{aligned} \sum_{\|k\|_\infty > N} \left| \widehat{G}_k \right| &\leq \left(\sum_{k \in \mathbb{Z}^3} \left| [\Delta^m (\widehat{G_\delta \chi})]_k \right|^2 \right)^{\frac{1}{2}} \left(\sum_{\|k\|_\infty > N} \frac{1}{\|k\|^{4m}} \right)^{\frac{1}{2}} \\ (5.2) \qquad \qquad \qquad &\leq cN^{\frac{3}{2}-2m} \|\Delta^m (G_\delta \chi)\|_{L^2} \end{aligned}$$

where the first step follows from the Cauchy-Schwarz inequality and the second step follows from Parseval's equation. Since the mollified Green's function gets more peaked in the origin as $\delta \rightarrow 0$ the norm of G_δ cannot be treated as a constant. Therefore N must be linked to δ . Unfortunately, the right-hand side in (5.2) involves the product of the Green's function with the cut-off function. The product rule leads to estimates that involve factors which depend on m and which are difficult to control.

Furthermore, the argument in (5.2) assumes that the cut-off function has the same regularity as G_δ , which, as numerical experiments suggest, is not necessary.

The following discussion presents a refined analysis intended to obtain more realistic error estimates.

5.1. Estimates of the Derivatives. Derivatives of the mollified Green's function can be obtained either from the Fourier transform (3.6) or the closed form (3.11). The Fourier integral leads to estimates that display the dependence on the order of differentiation more clearly. For the subsequent error analysis it suffices to work with powers of the Laplacian. Since the Bessel function satisfies the Helmholtz equation it follows from (3.6) that

$$(5.3) \quad \Delta^m G_\delta(r) = (-1)^m \int_0^\infty H\left(\delta(\rho^2 - \kappa^2)\right) \frac{\rho^{2+m}}{\rho^2 - \kappa^2} j_0(\rho\|r\|) d\rho$$

for any integer $m < q$. Because of the assumption (3.14), the filter decays only if the argument is larger than unity. This condition leads to

$$(5.4) \quad \delta(\rho^2 - \kappa^2) \geq 1 \Rightarrow \rho \geq \left(\frac{1}{\delta} + \kappa^2\right)^{\frac{1}{2}} =: \rho_0.$$

The definition of ρ_0 immediately implies that

$$(5.5) \quad \rho_0 = \frac{1}{\sqrt{\delta}} \sqrt{1 + \tilde{\kappa}^2},$$

i.e., $\rho_0 \leq c\kappa$.

LEMMA 5.1. *The following estimates hold*

$$(5.6) \quad |\Delta^m G_\delta(r)| \leq c \frac{m}{\|r\|} \left(\frac{1 + \tilde{\kappa}^2}{\delta}\right)^m,$$

$$(5.7) \quad \|\Delta^m G_\delta(r)\|_{L^2_{[-1,1]^3}} \leq cm \left(\frac{1 + \tilde{\kappa}^2}{\delta}\right)^m.$$

Proof. Break integral (5.3) into three parts

$$\Delta^m G_\delta(r) = \frac{(-1)^m}{2\pi^2} (I_1 + I_2 + I_3),$$

where

$$I_1 = \int_0^{\rho_0} \frac{f(\rho) - f(\kappa)}{\rho - \kappa} \frac{\rho^2}{\rho + \kappa} j_0(\rho\|r\|) d\rho,$$

$$I_2 = f(\kappa) \int_0^{\rho_0} \frac{\rho^2}{\rho^2 - \kappa^2} j_0(\rho\|r\|) d\rho,$$

$$I_3 = \int_{\rho_0}^\infty f(\rho) \frac{\rho^2}{\rho^2 - \kappa^2} j_0(\rho\|r\|) d\rho,$$

and

$$f(\rho) := \rho^{2m} H\left(\delta(\rho^2 - \kappa^2)\right).$$

Since $\delta\rho_0^2 \leq c$ the derivative of $f(\rho)$ is bounded by $|f'(\rho)| \leq cm\rho_0^{2m-1}$ for $0 \leq \rho \leq \rho_0$. Thus the first integral can be estimated as follows

$$\begin{aligned} |I_1| &\leq \max_{0 \leq \rho \leq \rho_0} |f'(\rho)| \int_0^{\rho_0} \frac{\rho^2}{\rho + \kappa} |j_0(\rho\|r\|)| d\rho \\ &\leq cm \frac{\rho_0^{2m-1}}{r} \int_0^{\rho_0} \frac{\rho}{\rho + \kappa} d\rho \\ (5.8) \quad &\leq cm \frac{\rho_0^{2m}}{\|r\|}. \end{aligned}$$

The integral in I_2 can be computed in closed form. The resulting expression involves the integral sine and cosine functions and are easily shown to be uniformly bounded, thus

$$(5.9) \quad |I_2| \leq c \frac{\kappa^{2m}}{\|r\|}.$$

The integration in I_3 is over the interval where the filter is decreasing. Therefore

$$\begin{aligned} |I_3| &\leq \frac{1}{\|r\|\delta^q} \int_{\rho_0}^{\infty} \frac{\rho^{2m+1}}{(\rho^2 - \kappa^2)^q} \frac{1}{\rho^2 - \kappa^2} d\rho \\ &\leq \frac{1}{\|r\|\delta^q} \max_{\rho_0 \leq \rho} \left| \frac{\rho^{2m+1}}{(\rho^2 - \kappa^2)^q} \right| \int_{\rho_0}^{\infty} \frac{1}{\rho^2 - \kappa^2} d\rho. \end{aligned}$$

The function to be maximized is monotonically decreasing; the integral can be computed in closed form and estimated by c/κ . Thus I_3 can be estimated by

$$(5.10) \quad |I_3| \leq \frac{c}{\kappa\|r\|} \rho_0^{2m+1}.$$

Estimate (5.6) is immediate from (5.5), (5.8), (5.9) and (5.10). Estimate (5.7) follows from (5.6) because the $1/r$ singularity cancels upon integration. \square

Using very similar arguments as in the previous proof, the first and second derivatives of powers of the Laplacian can be estimated. We only state the result.

LEMMA 5.2. *For $|\alpha| \leq 2$ we have*

$$(5.11) \quad \|\partial^\alpha \Delta^m G_\delta(r)\|_{L^2_{[-1,1]^3}} \leq c \frac{m}{\delta^{m+\frac{1}{2}}} (1 + \tilde{\kappa}^2)^{m+\frac{|\alpha|}{2}}.$$

5.2. Approximation Analysis of the Fourier Series. Our goal is an estimate the Fourier truncation error in the spirit of (5.2), that does not involve high-order derivatives of the cut-off function.

LEMMA 5.3. *If $\chi \in C^3$ then the Fourier coefficients of the kernel are given by*

$$\begin{aligned} \widehat{G}_k &= \frac{1}{\|k\|^{2m}} \left([\widehat{\Delta^m G_\delta}]_k + 2m [\widehat{\nabla \Delta^{m-1} G_\delta \cdot \nabla \chi}]_k \right) + \\ &\sum_{l=0}^{m-1} \frac{1}{\|k\|^{2l+2}} \sum_{\substack{|\alpha| \in \{1,2\} \\ |\beta| = 4-|\alpha|}} a_{\alpha,\beta}^l [\partial^\alpha \widehat{\Delta^{l-1} G_\delta} \partial^\beta \chi]_k \end{aligned}$$

for any integer m for which the right-hand side is defined. The coefficients satisfy $a_{\alpha,\beta}^l \in \{0, 1, 2l, 4l\}$.

Note that the above expression only contains derivatives of the cut-off function up to order three. Furthermore, the remainder (i.e., the sum over l), contains derivatives of G_δ which are at least two orders lower than the power of $1/\|k\|$. This will be essential for the subsequent error analysis.

Proof. A simple application of the product rule shows that

$$\begin{aligned}\Delta(G_\delta\chi) &= \Delta G_\delta\chi + 2\nabla G_\delta \cdot \nabla\chi + G_\delta\Delta\chi, \\ \Delta(\nabla G_\delta \cdot \nabla\chi) &= \nabla\Delta G_\delta \cdot \nabla\chi + 2\text{tr}(G_\delta''\chi'') + \nabla\chi \cdot \nabla\Delta G_\delta.\end{aligned}$$

From integration by parts it follows that

$$\widehat{G}_k = \frac{1}{\|k\|^2} [\widehat{\Delta(G_\delta\chi)}]_k = \frac{1}{\|k\|^2} \left([\widehat{\Delta G_\delta\chi}]_k + 2[\widehat{\nabla G_\delta \cdot \nabla\chi}]_k + [\widehat{G_\delta\Delta\chi}]_k \right).$$

Repeating this argument for the first two terms and leaving the third term unchanged leads to

$$\begin{aligned}\widehat{G}_k &= \frac{1}{\|k\|^4} \left([\widehat{\Delta^2 G_\delta\chi}]_k + 4[\widehat{\nabla\Delta G_\delta \cdot \nabla\chi}]_k \right) \\ &\quad + \frac{1}{\|k\|^4} \left([\widehat{\Delta G_\delta\Delta\chi}]_k + 4[\widehat{\text{tr}G_\delta''\chi''}]_k + 2[\widehat{\nabla G_\delta \cdot \nabla\Delta\chi}]_k \right) + \frac{1}{\|k\|^2} [\widehat{G_\delta\Delta\chi}]_k.\end{aligned}$$

By induction one finds that

$$\begin{aligned}\widehat{G}_k &= \frac{1}{\|k\|^{2m}} \left([\widehat{\Delta^m G_\delta\chi}]_k + 2m[\widehat{\nabla\Delta^{m-1}G_\delta \cdot \nabla\chi}]_k \right) \\ &\quad + \sum_{l=0}^{m-1} \frac{1}{\|k\|^{2l+2}} \left([\widehat{\Delta^l G_\delta\Delta\chi}]_k + 4l[\widehat{\text{tr}\Delta^{l-1}G_\delta''\chi''}]_k + 2l[\widehat{\nabla\Delta^{l-1}G_\delta \cdot \nabla\Delta\chi}]_k \right)\end{aligned}$$

which is the assertion. \square

Combining this result with the estimates of the derivatives of G_δ leads to the next theorem

THEOREM 5.4. *If $\chi \in C^3$, $f, g \in L^2(S)$ and N is chosen such that*

$$(5.12) \quad \lambda := \left(\frac{1 + \tilde{\kappa}^2}{\delta N^2} \right)^{\frac{1}{2}} < 1,$$

then for any integer $0 < m < q$ the approximation error of the truncated Fourier series is bounded by

$$|\langle f, (\mathcal{A} - \mathcal{A}_N)g \rangle| \leq c \left(m^2 N^{\frac{3}{2}} \lambda^m + N^{-\frac{1}{2}} \right) \|f\|_{L^2(S)} \|g\|_{L^2(S)}.$$

This theorem suggests how N must be selected to control the error as $\kappa \rightarrow \infty$. Recall that condition (3.15) implies that $\delta \sim 1/\kappa^2$ to ensure that $\tilde{\kappa}$ is bounded. Because of (5.12) one has to select N such that $N \sim 1/\sqrt{\delta}$. Since q is free, the product $N^{\frac{3}{2}}\lambda^m$ can always be controlled by letting q increase as N increases. The influence of q on the computational cost is negligible, therefore the error can be controlled with complexity $O(n + \kappa^3 \log \kappa)$.

Proof. Using the previous lemma it follows that

$$\begin{aligned} \sum_{\|k\|_\infty > N} |\widehat{G}_k| &\leq \sum_{\|k\|_\infty > N} \frac{1}{\|k\|^{2m}} \left| [\widehat{\Delta^m G_\delta}]_k + 2m [\nabla \Delta^{m-1} G_\delta \cdot \nabla \chi]_k \right| \\ &\quad + \sum_{l=0}^{m-1} \sum_{\substack{|\alpha| \in \{1,2\} \\ |\beta| = 4 - |\alpha|}} \sum_{\|k\|_\infty > N} \frac{1}{\|k\|^{2l+2}} |a_{\alpha,\beta}^l| \left| [\partial^\alpha \Delta^{l-1} G_\delta \partial^\beta \chi]_k \right|. \end{aligned}$$

Using Cauchy-Schwarz and Parseval in a similar manner that lead to estimate (5.2)

$$\begin{aligned} \sum_{\|k\|_\infty > N} |\widehat{G}_k| &\leq \frac{1}{N^{2m-\frac{3}{2}}} (\|\Delta^m G_\delta \chi\| + \|\nabla \Delta^{m-1} G_\delta \cdot \nabla \chi\|) \\ &\quad + \sum_{l=0}^{m-1} \frac{1}{N^{2l+\frac{1}{2}}} \sum_{\substack{|\alpha| \in \{1,2\} \\ |\beta| = 4 - |\alpha|}} |a_{\alpha,\beta}^l| \|\partial^\alpha \Delta^{l-1} G_\delta \partial^\beta \chi\|. \end{aligned}$$

The derivatives in the above expression can be estimated using the inequalities (5.7) and (5.11) derived in the previous section. Recalling the definition of λ in (5.12), this leads to

$$\sum_{\|k\|_\infty > N} |\widehat{G}_k| \leq cN^{\frac{3}{2}} m^2 \lambda^m + cN^{-\frac{1}{2}} \sum_{l=0}^{m-1} l^2 \lambda^l.$$

Since $\lambda < 1$ the sum is bounded independently of m . Combining the last inequality with (5.1) completes the proof. \square

6. Error Analysis of the non-equispaced FFT algorithm. The error analysis of the previous section is not complete since in the non-equispaced FFT algorithm the complex exponential function is approximated by the truncated Jacobi-Anger expansion. It is therefore important to know how the highest retained order p must be selected as a function of the wave number. This will be determined in this section.

6.1. Error of the multivariate Jacobi-Anger approximation. The Jacobi-Anger expansion is an expansion in Legendre polynomials. Therefore the error of the multi-variable truncated expansion in (4.8) is given by

$$(6.1) \quad \tilde{e}_k^p(t) := e_k(t) - \tilde{e}_k^p(t) = \sum_{n=p+1}^{\infty} \sum_{|\alpha|=n} e_\alpha L_\alpha(t)$$

where $e_k(t) = \exp(iH k \cdot t)$, \tilde{e}_k^p denotes the truncated expansion and the coefficient e_α has the form

$$e_\alpha = \int_{[-1,1]^3} e_k(t) L_\alpha(t) d^3t = \frac{(-1)^\alpha}{\alpha! 2^\alpha} \int_{[-1,1]^3} (1-t^2)^\alpha \partial^\alpha e_k(t) d^3t.$$

The latter form follows from the Rodrigues formula and integration by parts. It is useful for estimating the magnitude of the coefficient

$$|e_\alpha| \leq \frac{1}{\alpha! 2^\alpha} \int_{[-1,1]^3} (1-t^2)^\alpha d^3t \|\partial^\alpha e_k\|_\infty \leq \frac{1}{\alpha! 2^\alpha} (\pi H k)^\alpha.$$

Since $|L_n(t)| \leq 1$ for $|t| \leq 1$, the truncation error of (6.1) can be bounded as follows

$$\begin{aligned} |\widehat{e}_k^p(t)| &= \sum_{n=p+1}^{\infty} \sum_{|\alpha|=n} |e_\alpha|, \\ &\leq \sum_{n=p+1}^{\infty} \left(\frac{\pi H}{2}\right)^n \sum_{|\alpha|=n} \frac{|k^\alpha|}{\alpha!}, \\ &= \sum_{n=p+1}^{\infty} \left(\frac{\pi H}{2}\right)^n \frac{\|k\|_1^n}{n!}. \end{aligned}$$

The last step is an application of the multivariate binomial formula. Since the last equation is the remainder of the Taylor expansion of the exponential function, we have the bound

$$(6.2) \quad \|\widehat{e}_k^p\|_{L^\infty_{[-1,1]^3}} \leq \frac{c}{(p+1)!} \left(\frac{\pi}{4N}\|k\|_1\right)^{p+1}.$$

If in (6.1) the Taylor series instead of the Jacobi-Anger is employed, then a very similar analysis shows that

$$\|\widehat{e}_k^p\|_{L^\infty_{[-1,1]^3}} \leq \frac{c}{(p+1)!} \left(\frac{\pi}{2N}\|k\|_1\right)^{p+1}.$$

Thus the Jacobi-Anger expansion is significantly more accurate for large values of k .

6.2. Error of the non-equispaced FFT. In the non-equispaced FFT algorithm, the kernel G_N in (4.2) is replaced by the kernel

$$(6.3) \quad G_N^p(x, x') = \sum_{\|k\|_\infty \leq N} \widehat{G}_k \exp\left(i\pi \frac{k \cdot (l - l')}{N}\right) \tilde{e}_k(t_l) \tilde{e}_k(t_{l'}), \quad x \in C_l, x' \in C_{l'}$$

where $t_l = (x - x_l)/H$, $t_{l'} = (x' - x_{l'})/H$. Thus the error is given by

$$\begin{aligned} G_N(x - x') - G_N^p(x, x') &= \\ &\sum_{\|k\|_\infty \leq N} \widehat{G}_k \exp\left(i\pi \frac{k \cdot (l - l')}{N}\right) \left(\widehat{e}_k(t_l) \tilde{e}_k(t_{l'}) + \tilde{e}_k(t_l) \widehat{e}_k(t_{l'}) + \widehat{e}_k(t_l) \widehat{e}_k(t_{l'})\right). \end{aligned}$$

From (6.2) and $\|k\|_1 \leq \sqrt{3}\|k\|$ the estimate

$$(6.4) \quad \left|G_N(x - x') - G_N^p(x, x')\right| \leq \frac{c}{(p+1)!} \left(\frac{\sqrt{3}\pi}{4N}\right)^{p+1} \sum_{\|k\|_\infty \leq N} \left|\widehat{G}_k\right| \|k\|^{p+1}$$

follows. We use the identity

$$\widehat{G}_k = \frac{[\widehat{\Delta^2(G\chi)}]_k}{\|k\|^4}$$

and recall that from Section 5 it follows that

$$\|\Delta^2(G_\delta\chi)\|_{L^2} \leq c\delta^{-2}.$$

Continuing with estimate (6.4) gives

$$\begin{aligned}
& \left| G_N(x - x') - G_N^p(x, x') \right| \\
& \leq \frac{c}{(p+1)!} \left(\frac{\sqrt{3}\pi}{4N} \right)^{p+1} \left(\sum_{\|k\|_\infty \leq N} \|k\|^{2p-6} \right)^{\frac{1}{2}} \left(\sum_{\|k\|_\infty \leq N} \left| [\widehat{\Delta^2(G\chi)}]_k \right|^2 \right)^{\frac{1}{2}} \\
(6.5) \quad & \leq \frac{c}{(p+1)!} \left(\frac{\sqrt{3}\pi}{4} \right)^{p+1} N^{-\frac{1}{2}} (\delta N^2)^2.
\end{aligned}$$

We have almost completed the proof of the following theorem

THEOREM 6.1. *Let \mathcal{A}_N^p the integral operator that has kernel G_N^p then*

$$|\langle f, (\mathcal{A}_N - \mathcal{A}_N^p)g \rangle| \leq \frac{c}{(p+1)!} \left(\frac{\sqrt{3}\pi}{4} \right)^{p+1} N^{-\frac{1}{2}} \|f\|_{L^2(S)} \|g\|_{L^2(S)}.$$

The most important conclusion from this result is that the order p in the Jacobi-Anger approximation does not have to be increased as $N \rightarrow \infty$.

Proof. Elementary integral calculus and estimate (6.5) together with the fact that $\delta \sim N^{-2}$ imply that

$$\begin{aligned}
|\langle f, (\mathcal{A}_N - \mathcal{A}_N^p)g \rangle| & \leq \max_{x, x' \in S} |G_N(x - x') - G_N^p(x, x')| \|f\|_{L^1(S)} \|g\|_{L^1(S)} \\
& \leq \frac{c}{(p+1)!} \left(\frac{\sqrt{3}\pi}{4} \right)^{p+1} N^{-\frac{1}{2}} \|f\|_{L^2(S)} \|g\|_{L^2(S)}.
\end{aligned}$$

□

7. Numerical Examples. We have implemented the method to verify the theoretical estimates. In this implementation the Fourier coefficients are computed numerically. The method used for this task is completely analogous to the computation of the Fourier coefficients of a surface density described in Section 4.1. The only difference is that the moments in (4.9) are replaced by the moments of the Green's function

$$m_l^\alpha(G) = \int_{C_l} P_\alpha\left(\frac{y - x_l}{H}\right) G_\delta(y) \chi(y) d^3y$$

where $C_l = x_l + H[-1, 1]^3$. These moments are computed using Gauss quadrature. The analysis of the error introduced by computing \widehat{G}_k numerically parallels the discussion of Section 6.2 and is therefore omitted.

In the first example we compute the farfield pattern when the unit sphere is hit with a plane wave. This is done by solving integral equation (2.6) with piecewise constant elements combined with the spectral method. The farfield is computed from the density using the formula

$$\alpha(\widehat{x}) = i \int_S \exp(-i\kappa\widehat{x} \cdot y) (\eta + \kappa\widehat{x} \cdot n_y) \sigma(y) dS_y, \quad \widehat{x} \in \mathbb{S},$$

see, e.g., [12]. Because of the spherical symmetry the solution σ as well as the farfield can be expressed in closed form. The coupling parameter in (2.3) is $\eta = \kappa/2$ and the

linear system is solved with GMRES without any preconditioning. Tables 7.1 and 7.1 display the relative errors of the L_2 -norm of $\alpha(\hat{x})$ when increasing the size of the sphere measured in wavelengths. The results show that the error remains bounded (actually, decreases somewhat) when $N \sim \kappa$ and $\delta \sim 1/\kappa^2$ and are therefore in good agreement with the theoretical estimates. The truncation parameter of the Jacobi-Anger expansion in (6.1) is always set to $p = 4$. In these experiments the meshwidth is proportional to the wavelength, which is reflected in the fact that the number of panels n is quadrupled in every line. We have implemented both filters (3.16) and (3.17) and set $q = 5$. The displayed results are for (3.17), but the results for the other filter are only marginally different. The timings displayed are the time per iteration and the total time, which also includes the time to compute the Fourier coefficients \widehat{G}_k . The cpu is a 3.6 ghz Intel Xeon processor. The time per iteration increase by a factor somewhat larger than eight when doubling the wavenumber, which agrees well with the $\kappa^3 \log \kappa$ complexity estimate. The code stores the Fourier coefficients \widehat{G}_k and \widehat{g}_k , the moments $m^\alpha(g)$, and as well as the orthogonal basis of the Krylov subspace generated by GMRES. For the size of problems computed, the basis consumes the largest portion of the overall memory usage. Since this part grows roughly like κ^2 , the growth rate of the overall storage appears slower in the Table than the asymptotic $\kappa^3 \log \kappa$ estimate.

| n | N | size (λ) | δ | its | mem (MB) | time/itr (sec) | time (sec) | error |
|---------|-----|-----------------------|-----------------------|-----|-------------|-------------------|---------------|-------|
| 5120 | 16 | 6.25 | 1.00×10^{-4} | 11 | 8.0 | 0.4 | 5 | 0.076 |
| 20480 | 32 | 12.5 | 2.50×10^{-5} | 12 | 32.8 | 2.1 | 32 | 0.044 |
| 81920 | 64 | 25 | 6.25×10^{-6} | 15 | 139.8 | 18.3 | 337 | 0.039 |
| 327680 | 128 | 50 | 1.56×10^{-6} | 18 | 623.9 | 159.2 | 3355 | 0.034 |
| 1310720 | 256 | 100 | 3.91×10^{-7} | 22 | 2981.7 | 1386 | 34414 | 0.031 |

TABLE 7.1

Results for the sphere. Lower accuracy.

| n | N | size (λ) | δ | its | mem (MB) | time/itr (sec) | time (sec) | error |
|---------|-----|-----------------------|-----------------------|-----|-------------|-------------------|---------------|--------|
| 5120 | 16 | 3.13 | 1.00×10^{-4} | 8 | 8.0 | 0.4 | 5 | 0.044 |
| 20480 | 32 | 6.25 | 2.50×10^{-5} | 11 | 32.8 | 2.2 | 32 | 0.021 |
| 81920 | 64 | 12.5 | 6.25×10^{-6} | 12 | 139.8 | 17.9 | 276 | 0.011 |
| 327680 | 128 | 25 | 1.56×10^{-6} | 15 | 623.9 | 159.3 | 2880 | 0.0071 |
| 1310720 | 256 | 50 | 3.91×10^{-7} | 18 | 2981.7 | 1378 | 28714 | 0.0051 |

TABLE 7.2

Results for the sphere. Higher accuracy.

To illustrate that the technique discussed in this paper can be used for very general scatterers we include the Boeing 747 example shown in Figure 7.1. The surface of the airplane is assumed to be sound soft. The geometry is given by a list of vertices and triangular panels which can be downloaded from the internet. There are 556552 panels, and further information, such as parameterizations, are known. We ignore the fact that there are edges and conical vertices in the geometry and set the curvature term in (3.24) to zero.

Figure 7.2 compares the density for $N = 128$ and $N = 256$ Fourier modes.



FIG. 7.1. 3D rendering of the airplane.

Since it is hard to spot differences in the two solutions, it appears that already the smaller value of N will give an acceptable accuracy in many applications. The size of the scatterer in this problem is about 45 wavelengths, the memory allocation of the smaller problem is 906MB and the cpu time is 4355 seconds.

Figure 7.3 displays the solution for 90 wavelengths and $N = 256$. The memory allocation is 1583 MB and the cpu time is 36361 seconds.

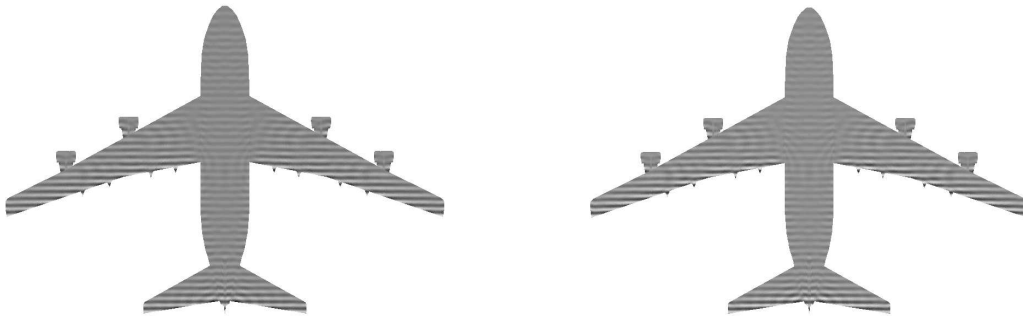


FIG. 7.2. Comparison of the density (imaginary part) for $N = 128$ (left) with $N = 256$ (right); 45 wavelengths

8. Conclusions. We have presented a method for the computation of scattered fields that has $O(\kappa^3 \log \kappa)$ complexity when the meshwidth is proportional to the wavelength. Since $n \sim \kappa^2$ the asymptotic estimate is not optimal, but because of small constants we have been able to solve 100λ -problems in eight to nine hours. Most of the cpu time is spent evaluating the sums in (4.10) and (4.11). Since this part is em-



FIG. 7.3. *The density (imaginary part) for 90 wavelengths*

barrasingly parallel one can expect almost optimal speed up on distributed memory multiprocessor machines. The approach generalizes to electromagnetic scattering.

9. Acknowledgement. The author obtained the panel description file of the airplane from the website www.3dcafe.com.

REFERENCES

- [1] G. Beylkin, R. Coifman, and V. Rokhlin. Fast wavelet transforms and numerical algorithms. *Comm. Pure Appl. Math.*, XLIV:141–183, 1991.
- [2] S. Börm, L. Grasedyck, and W. Hackbusch. Introduction to hierarchical matrices with applications. *Engrg. Anal. Boundary Elements*, pages 405 – 422, 2002.
- [3] H. Brakhage and P. Werner. über das Dirichletsche Aussenraumproblem für die Helmholtzsche Schwingungsgleichung. *Arch. Math.*, 16:325–329, 1965.
- [4] O. Bruno and L. Kunyansky. A fast, high-order algorithm for the solution of surface scattering problems: Basic implementation, tests, and applications. *J. Comput. Phys.*, 169(1):80–110, May 2001.
- [5] D. Colton and R. Kress. *Integral Equation Methods in Scattering Theory*. Wiley, New York, 1983.
- [6] E. Darve. The fast multipole method I: Error analysis and asymptotic complexity. *SIAM J. Numer. Anal.*, 38(1):98–128, 2000.
- [7] D.G. Duffy. *Green's Functions with Applications*. Chapman and Hall/CRC, 2001.
- [8] M. Ganesh and I.G. Graham. A high-order algorithm for obstacle scattering in three dimensions. *J. Comput. Phys.*, 198:211–242, 2004.
- [9] L. Greengard and V. Rokhlin. A fast algorithm for particle simulations. *J. Comput. Phys.*, 73:325–348, 1987.
- [10] L. Greengard and J. Strain. A fast algorithm for the evaluation of heat potentials. *Comm. Pure Appl. Math.*, XLIII:949–963, 1990.
- [11] R. W. Hockney and J. W. Eastwood. *Computer Simulations using Particles*. McGraw-Hill, New York, 1988.

- [12] J-C. Nédélec. *Acoustic and Electromagnetic Equations*. Springer, 2001.
- [13] A.P. Peirce and J.A.L. Napier. A spectral multipole method for efficient solution of large-scale boundary element models in elastostatics. *Internat. J. Numer. Methods Engrg.*, 38:4009–4034, 1995.
- [14] J. Phillips and J. White. A precorrected-FFT method for electrostatic analysis of complicated 3-D structures. *IEEE Trans. Circuits and Systems*, 16(10):1059–1073, 1997.
- [15] V. Rokhlin. Rapid solution of integral equations of scattering theory in two dimensions. *J. Comput. Phys.*, 86:414–439, 1990.
- [16] S.A. Sauter. Variable order panel clustering. *Computing*, 64(3):223–277, May 2000.
- [17] R. Schneider. *Multiscalen- und Wavelet- Matrixkompression: Analysisbasierte Methoden zur effizienten Loesung grosser vollbesetzter Gleichungssysteme*. Teubner, Stuttgart, 1998.
- [18] J.M. Song, C.C. Lu, W.C. Chew, and S.W. Lee. Fast Illinois solver code FISC. *IEEE Antennas Propag. Mag.*, 40:27–34, 1998.
- [19] J. Tausch. The variable order fast multipole method for boundary integral equations of the second kind. *Computing*, 72(3):267 – 291, 2004.